small methods
www.small-methods.com

Spherical Micro/Nano Hierarchical Structures for Energy and Water Harvesting Devices

Young Jung, Junseong Ahn, Ji-Seok Kim, Ji-Hwan Ha, Jaehwan Shim, Hanchul Cho, Yong Suk Oh, Yong-Jin Yoon, Youngsuk Nam, Il-Kwon Oh, Jun-Ho Jeong, and Inkyu Park**

Three-dimensional (3D) hierarchical structures have been explored for various applications owing to the synergistic effects of micro- and nanostructures. However, the development of spherical micro/nano hierarchical structures (S-HSs), which can be used as energy/water harvesting systems and sensing devices, remains challenging owing to the trade-off between structural complexity and fabrication difficulty. This paper presents a new strategy for facile, scalable S-HS fabrication using a thermal expansion of microspheres and nanopatterned structures. When a specific temperature is applied to a composite film of microspheres and elastomers with nanopatterned surfaces, microspheres are expanded and 3D spherical microstructures are generated. Various nanopatterns and densities of spherical microstructures can thereby be quantitatively controlled. The fabricated S-HSs have been used in renewable electrical energy harvesting and sustainable water management applications. Compared to a triboelectric nanogenerator (TENG) with bare film, the S-HS-based TENG exhibited 4.48 times higher triboelectric performance with high mechanical durability. Furthermore, an S-HS is used as a water harvesting device to capture water in a fog environment. The water collection rate is dramatically enhanced by the increased surface area and locally concentrated vapor diffusion flux due to the spherical microstructures.

1. Introduction

Three-dimensional (3D) hierarchical structures observed in nature have attracted significant attention in recent times owing to their advanced and diverse practical applications in surface physics.[1,2] The combination of different scales and features of components in these structures can engender a synergistic effect on the physicochemical properties of the entire structure and the outstanding properties of their constitutive building blocks. For example, inspired by the 3D hierarchical structure of the gecko's feet, which enables them to climb various textured surfaces, such as concrete and glass, surfaces with strong adhesion have been widely used.[3,4] In addition, the micro/nanoscale hierarchical structures inspired by the lotus plant, which impart self-cleaning properties, prevent the adhesion of rain on windows, antennas, and solar cells, thereby maintaining their performance in harsh environments.[5] Research on the micro/nano hierarchical structures has facilitated their applications to chemical sensors,[6] fuel cells,[7] and self-cleaning systems[8] owing to their increased surface areas and roughness. In particular, micro/nano hierarchical structures are suitable for these applications because they bolster the advantages of micro- and nanostructures. Typically, microstructures can be used to adjust mechanical properties such as the hardness and elastic modulus.[9] Nanostructures also exhibit characteristics such as hydrophobicity and increased surface area.[10,11] Well-designed and adjustable micro/nano hierarchical structures can be applied to harvesting systems, such as triboelectric generators and water harvesting devices with high performance through controlled mechanical properties and increased surface area.[12,13] Therefore, it is essential to fabricate well-designed hierarchical structures that can be manufactured by means of a low-cost process for applications in engineering fields.

Several methods have been suggested for manufacturing micro/nano hierarchical structures on surfaces, including semiconductor fabrication processes,[14] molding and imprinting,[15] chemical synthesis,[16] and etching.[17] In particular, various methods have been proposed for fine-tuning the geometric features at different levels with high precision. For example, Tian et al. proposed hierarchically ordered structures using an electrohydrodynamic structure formation method based on a prestructured polymer under an applied electric field.[18] Lin et al. proposed superhydrophobic surfaces based on hierarchical structures using two-photon polymerization.[19] These methods are effective for fabricating complex micro/nano hierarchical structures on flexible substrates. However, these

Y. Jung, J. Ahn, J.-S. Kim, J.-H. Ha, J. Shim, Y. S. Oh, Y.-J. Yoon, Y. Nam, I.-K. Oh, I. Park
Department of Mechanical Engineering
Korean Advanced Institute of Science and Technology (KAIST)
Daejeon 34141, Republic of Korea
E-mail: inkyu@kaist.ac.kr
J. Ahn, J.-H. Ha, J.-H. Jeong
Department of Nano Manufacturing Technology
Korea Institute of Machinery and Materials (KIMM)
Daejeon 34103, Republic of Korea
E-mail: jhjeong@kimm.re.kr
H. Cho
Precision Mechanical Process and Control R&D Group
Korea Institute of Industrial Technology (KITECH)
Busan 46938, Republic of Korea
The ORCID identification number(s) for the author(s) of this article can be found under https://doi.org/10.1002/smtd.202200248.

DOI: 10.1002/smtd.202200248

© 2022 Wiley-VCH GmbH

Check for updates
23669608, 2022, 7, Downloaded from https://onlinelibrary.wiley.com/doi/10.1002/smtd.202200248 by Korea Advanced Institute Of, Wiley Online Library on [21/11/2022]. See the Terms and Conditions (https://onlinelibrary.wiley.com/terms-and-conditions) on Wiley Online Library for rules of use; OA articles are governed by the applicable Creative Commons License

approaches suffer from high manufacturing costs and poor scalability. Furthermore, fabricated secondary nanostructures only cover the top surfaces of the primary microstructures; no secondary nanostructures can be created on their sidewalls or in their valleys using these methods. Fully covering the secondary nanostructures on the primary microstructures is desirable in many applications considering that the degree of coverage can influence various physical and chemical properties of the structured surface. However, the development of a simple and low-cost fabrication process of micro/nano hierarchical structures with fully covered secondary nanostructures remains challenging.

To address this issue, we propose a new strategy for the facile and scalable fabrication of spherical micro/nano hierarchical structures (S-HSs) using the nanopatterned structures and thermally expandable microspheres. For the hierarchical structure to be employed in practical applications, the following three features are considered: i) full coverage of the secondary nanostructures on the primary microstructures, ii) high-throughput and low-cost fabrication process, and iii) easy control of geometrical variables such as shape, size, and density of micro/nano-structures. S-HSs with spherical primary microstructures and well-defined nanostructures were directly fabricated in this study by combining the nanopatterned structures and thermally expandable microspheres. This hierarchical structure, which enables control of the various types of nanopatterns and the density of spherical microstructures, dramatically increases the surface area and roughness of the structure. A numerical simulation was conducted to predict the final shape and location of the nanopatterns by the microsphere expansion, showing a close matching with the experimental data. Using these hierarchical structures, effective energy and water harvesting devices, namely, a triboelectric nanogenerator (TENG) and a water harvesting device were obtained. The developed TENG based on hierarchical structures exhibited high performance, mechanical durability, and required low fabrication cost. Also, the developed water harvesting device based on hierarchical structures showed a superior water collection rate as compared to that of bare film.

2. Results and Discussion

2.1. Concept and Fabrication Process of S-HSs

The fabrication of the S-HS using the proposed method of combining the nanoimprinting process, and thermally expandable microspheres is illustrated in **Figure 1**a. The nanoimprinting process involves the rapid, cost-effective transfer of specific nanopatterns from a master mold to an elastomer substrate. This method has been extensively used by various research groups owing to its fabrication advantages, such as high reproducibility, reusability, and scalability. Thermally expandable microspheres are widely used as packaging, fillers, and blowing agents because of their expandability and scalability. Microspheres can be easily dispersed in solvents (acetone, ethanol, and isopropyl alcohol) and mixed with various types of elastomers; randomly distributed spherical structures can thus be manufactured on a large scale. We designed a new type of S-HS by combining these two essential processes. The proposed approach enables not only the fabrication of various nanopatterns but also the quantitative control of the density of the primary microstructures. Figure 1b shows the mechanism of microsphere expansion. The microspheres consist of thermoplastic resins (acrylonitrile (AN) copolymers) at the outer shell and liquid hydrocarbon at the inside core (Figure 1b(i)). When the microspheres are heated to a specific temperature, the AN copolymer shell softens, and the hydrocarbon inside the core changes from liquid to gas (Figure 1b(ii)). The gasified hydrocarbon then begins to diffuse into the composites through the thin outer shell, the microspheres expand three to six times their initial volume (Figure 1b(iii)).

Figure 1c shows the measured size distributions of the microspheres. In the initial state, the average and standard deviation of the microspheres' diameters were measured as 14.1 ± 2.6 μm. When heat was applied to the microspheres, they began to expand, and the average size rapidly increased with temperature. The average and standard deviation of the microspheres' diameters were increased to 57.3 ± 9.1 μm after thermal expansion at 180 °C, where the microsphere expansion was maximized. After expansion, microspheres maintained their shapes at room temperature and cool down condition due to plastic deformation of the outer shell. However, as the temperature rose above 200 °C, the microspheres shrank owing to polymer degradation near the melting point, and the overall diameter of the microspheres gradually decreased (Figure S1, Supporting Information). Figure 1d schematically illustrates the fabrication process of the S-HS via the combination of the nanopatterned structures and thermally expandable microspheres. Firstly, we prepared a nanopatterned mold, which created uniform nanopatterns, and then treated it with a self-assembled monolayer for easy detachment of the replicated polydimethylsiloxane (PDMS) from the mold (Figure 1d(i)). Then, the PDMS/microsphere precursor was poured into the nanopatterned mold and thermally cured (Figure 1d(ii)). Pressure was applied to the mixture using a hand roller to facilitate the complete penetration into the nanopatterns of the mold (Figure 1d(iii)). The cured PDMS/microsphere composite was then separated from the mold (Figure 1d(iv)). The microspheres were mixed with the elastomer to fabricate a composite film, which contained nanopatterns on the surfaces before expansion (Figure 1d(v)). When heat was applied to the PDMS/microsphere composite, spherical microstructures were generated throughout the surface (Figure 1d(vi)).

2.2. Observation of S-HSs Surface

As mentioned above, the proposed fabrication method enables the manufacturing of various types of secondary nanostructures. **Figure 2** shows field emission scanning electron microscopy (FE-SEM) images and observation results of the S-HS surface with different nanopatterns. To illustrate the fact that the S-HS could be fabricated, low-magnification images of the primary microstructures are shown in Figure 2a. The line pattern with a linewidth (W) of 1 μm was formed on the spherical microstructures. The nanopatterns on top of the spherical microstructures were distorted into curved patterns with the

© 2022 Wiley-VCH GmbH

23669608, 2022, 7, Downloaded from https://onlinelibrary.wiley.com/doi/10.1002/smtd.202200248 by Korea Advanced Institute Of, Wiley Online Library on [21/11/2022]. See the Terms and Conditions (https://onlinelibrary.wiley.com/terms-and-conditions) on Wiley Online Library for rules of use; OA articles are governed by the applicable Creative Commons License

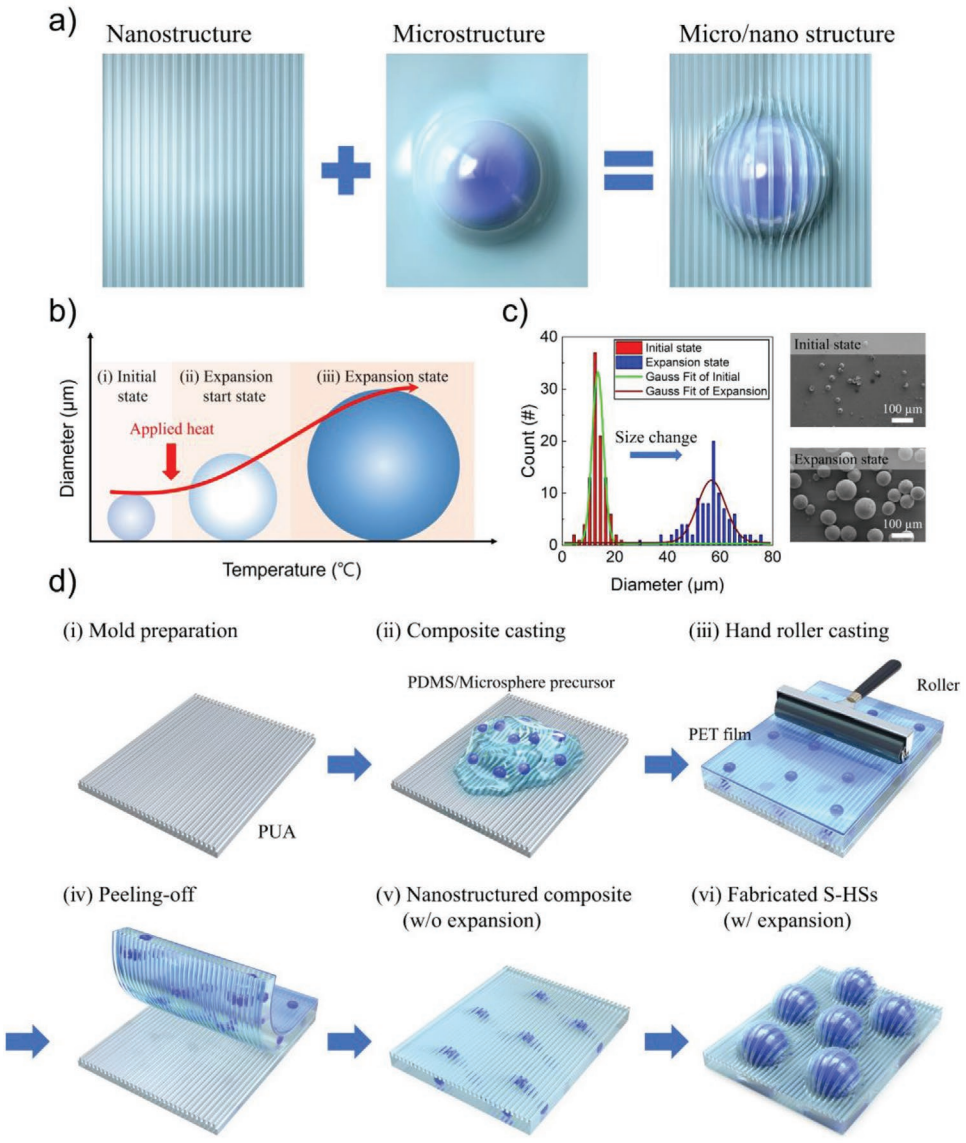


Figure 1. Spherical micro/nano hierarchical structure (S-HS) concept and fabrication process. a) Schematic of the S-HS concept. b) Expansion mechanism of thermally expandable microsphere. c) Size distribution and field emission scanning electron microscopy (FE-SEM) images of the microspheres before and after thermal expansion. The size of the microspheres changed with the applied temperature. d) Fabrication process of the S-HS based on nanopatterned molds, and thermal expansion of microspheres.

expansion of the microsphere. On the other hand, the nanopattern was maintained in other areas. The 3D profile of the spherical hierarchical structure with the line patterns was measured using a confocal laser microscope (Figure 2b). Figure 2c shows the cross-sectional profiles along specific lines (AA'). In the case of AA' (the vertical direction), the line patterns were clearly observed along the 3D surface of the spherical microstructure. Six types of nanopatterns (two types of line patterns, a hexagonal mesh, square mesh, square pillar, and cross mesh) were fabricated on the polyurethane acrylate (PUA) film and the mixture of PDMS precursor and microspheres was poured on the nanopatterned PUA mold and cured (Figure 2d). The size details and FE-SEM images of the nanopatterned molds are presented in Table S1 and Figure S2 (Supporting Information). In the case of the nanoline pattern with $W = 200$ nm, the shape of the pattern was slightly blurred compared to those of the other patterns. This result can be explained by the depth of the nanopattern and the high expandability of the microspheres. In the case of the nanoline pattern with $W = 200$ nm, the pattern and depth were narrow, at 200 and 400 nm, respectively. Hence, it was difficult for the PDMS/microsphere precursor with high viscosity to completely fill the PUA mold. In addition, the high expandability of the microsphere caused deformation of the pattern in the vertical direction. For other patterns, secondary nanopatterns were clearly observed and distinguished on the thermally expanded surface.

This method facilitated an effective control over the weight percentage of microspheres through the addition of

© 2022 Wiley-VCH GmbH

23669608, 2022, 7, Downloaded from https://onlinelibrary.wiley.com/doi/10.1002/smtd.202200248 by Korea Advanced Institute Of, Wiley Online Library on [21/11/2022]. See the Terms and Conditions (https://onlinelibrary.wiley.com/terms-and-conditions) on Wiley Online Library for rules of use; OA articles are governed by the applicable Creative Commons License

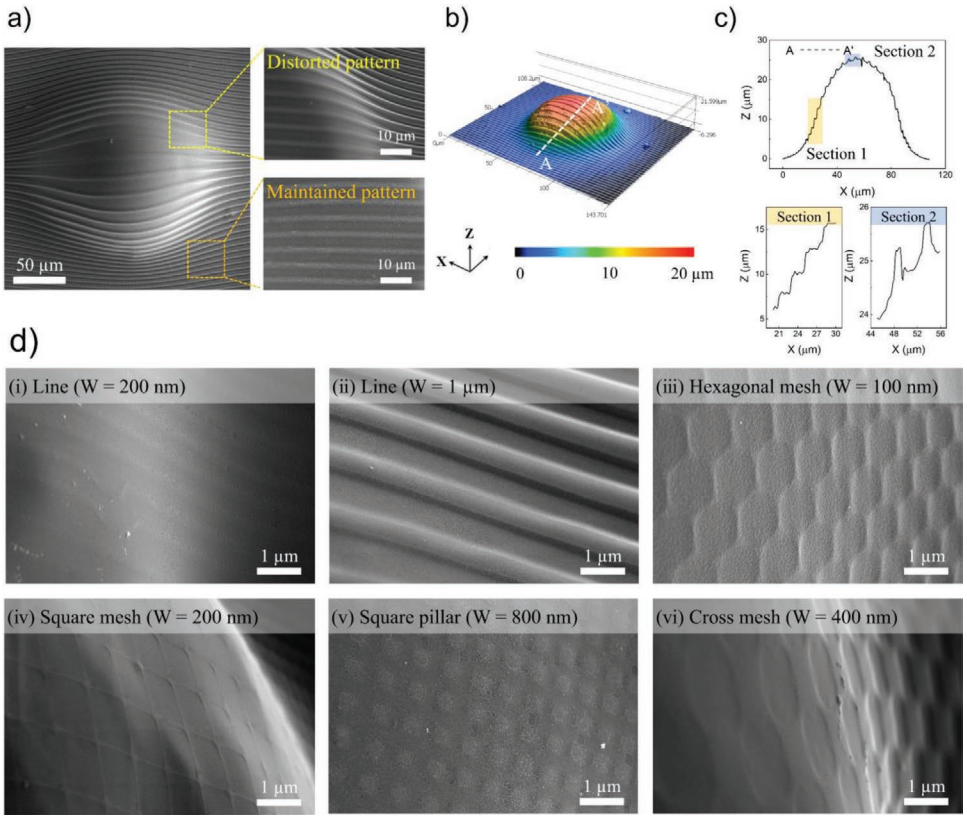


Figure 2. Field emission scanning electron microscopy (FE-SEM) images of the spherical micro/nano hierarchical structure (S-HS) surface for different nanopatterns. a) Line pattern with a line width of 1000 nm formed on the spherical microstructure by microsphere expansion. b) Three-dimensional (3D) profile measurement results of the S-HS. c) Cross-sectional profiles along specific lines (AA') to verify the nanopatterns. d) FE-SEM images of the transferred nanopatterns on the microstructures.

microspheres to the elastomer. Thus, the density of the primary microstructure caused by the expansion of the microspheres could be quantitatively controlled. **Figure 3** shows the FE-SEM images and measured roughness parameters of the S-HS surface for different concentrations of thermally expandable microspheres. To use S-HS effectively in various energy/water harvesting devices, it is important to control the primary microstructures that can significantly affect the elastic modulus and surface areas quantitatively. We measured the density (area fraction) of S-HS according to the microsphere concentration and analyzed the primary microstructures on the surface. To observe the surface according to the microsphere concentration, we fabricated various concentrations of S-HS (5, 10, 15, and 20 wt%) and observed the surface using FE-SEM (Figure 3a). The area fraction of the surface was calculated using the threshold function of the ImageJ program (Figure S3, Supporting Information). The S-HS with a microsphere concentration of 5 wt% had a slight microstructure on the surface, and the area fraction of the surface per unit area was calculated to be only 10.2 ± 2.2%. As the microsphere concentration increased, the area fraction significantly increased to 29.5 ± 5.7% and 71.9 ± 15.1% for 10 and 20 wt%, respectively (Figure 3b). In addition, the surface profiles of the S-HSs were measured, as shown in Figure 3c. At 5 and 10 wt% of the microsphere concentration, the maximum heights on the S-HS were measured as 15.6 and 25.4 μm. On the other hand, for 15 and 20 wt% concentration of microspheres, the overall size increased by the aggregation of the microsphere, and much larger microstructures as 45.2 and 71.9 μm were observed. In particular, the microsphere aggregation occurred for 15 and 20 wt%, while the nanopatterns were well-maintained on the surface (Figure S4, Supporting Information). To verify the changed microstructure size, two roughness parameters (arithmetical mean height and maximum height) were measured using a confocal laser microscope (Figure 3d). The average height increased with the microsphere concentration. On the other hand, the maximum height was almost the same in the 5 and 10 wt% cases, whereas from 15 wt%, it increased significantly due to the aggregation of microspheres. These results confirm that not only the density but also the height of the microstructure can be effectively controlled by adjusting the concentrations of microspheres.

2.3. Size Distribution and Simulation of Microstructures with Nanopatterns

The proposed S-HS has advantages with respect to its easy fabrication process, scalability, and controlled surface areas according to the types of nanopatterns and microstructure density. However, the microspheres buried inside the elastomer and nanopatterns formed on the surface can affect the expansion properties, that is, the size and shape of the microstructures.

© 2022 Wiley-VCH GmbH

23669608, 2022, 7, Downloaded from https://onlinelibrary.wiley.com/doi/10.1002/smtd.202200248 by Korea Advanced Institute Of, Wiley Online Library on [21/11/2022]. See the Terms and Conditions (https://onlinelibrary.wiley.com/terms-and-conditions) on Wiley Online Library for rules of use; OA articles are governed by the applicable Creative Commons License

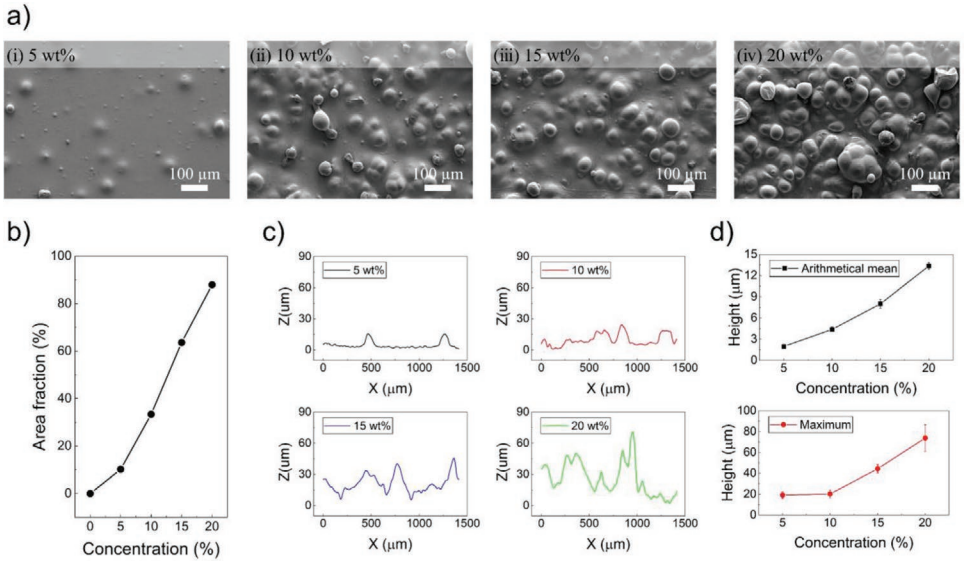


Figure 3. Field emission scanning electron microscopy (FE-SEM) images and measured roughness parameters of the spherical micro/nano hierarchical structure (S-HS) surface for various densities of thermally expandable microspheres. a) Surface of the S-HS according to the microsphere concentration. As the microsphere concentration increased, a large amount of microstructure was generated on the surface. b) Area fraction calculated based on FE-SEM images. c) Surface profile measurement of S-HSs. d) Arithmetic mean height and maximum height measurement results.

We checked the size of the microstructures of the S-HS with various types of nanopatterns, as shown in **Figure 4**a (bare; line pattern with $W = 1$ μm; hexagonal mesh; square pillar). The average diameters and standard deviations of bare, line, hexagonal mesh, and square pillar patterns were measured as 21.2 ± 6.5, 22.4 ± 7.4, 19.3 ± 7.3, and 19.9 ± 4.1 μm, respectively. The size of the microstructures was observed to be smaller than that measured under air conditions because the microsphere was buried inside the elastomer during the thermal expansion process. We further investigated the expansion size using the approximated Gaussian distribution in Figure 4b. In the case of the composite film mixed with the elastomer, the four types of nanopatterns exhibited approximately identical tendencies, indicating high reproducibility in the fabrication process with negligible deviations. These results demonstrate that the nanopatterns do not constrain the expansion of microspheres and affect the fabrication of primary microstructures. In addition, the uniformity of S-HS is one of the important factors for obtaining high performance devices with high degree of reproducibility. We checked the uniformity by the following two tests: comparison of size distribution of spherical microstructures (i) between multiple regions in a single sample and (ii) between multiple samples. They exhibited similar tendencies with negligible deviations, indicating high uniformity and reproducibility in the fabrication process with negligible deviations (Figure S5, Supporting Information). The changed distance (i.e., pitch) between the periodic nanopatterns after thermal expansion of the microspheres was calculated using the numerical simulation and FE-SEM image analysis. As shown in Figure 4c, the pitch of the periodic nanopatterns in the center region of the microspheres was expanded to approximately 3.9 times the original value, whereas the pitch in the side region of the microspheres was contracted to approximately 0.8 times its original value. These numerical simulation results well match the experimental results, as shown in Figure 4d, which means that the final shape and pitch distribution of the nanopatterns can be precisely predicted by the simulation.

2.4. Application of S-HS to Renewable Mechanical Energy Harvesting

To demonstrate the broad applicability of the developed S-HS, it was used for energy and water harvesting. As the public concern regarding issues associated with the climate changes, such as global warming and drought, has escalated in recent years, many studies on the use of renewable energy harvesting and sustainable water harvesting to solve these problems have been conducted.[20] We propose two types of harvesting systems to help address the environmental issues: i) TENGs for renewable electrical energy harvesting and ii) water harvesting systems to capture water in fog environments for sustainable water harvesting. Firstly, TENGs are of great interest because they can harvest renewable energy by converting wasted mechanical energy into electrical energy. They have the advantage of high efficiency in the harvesting of low-frequency mechanical motions, such as ocean waves, wind, and human motion.[21] To use TENGs effectively for the actual harvesting of wasted mechanical energy, three key objectives—high performance for efficient energy harvesting, high mechanical durability under applied pressure for sustainable energy harvesting, and high throughput and a low fabrication cost—should be considered.[22] To realize these objectives, researchers have developed various methods, such as applying micro- or nanopatterning to enhance the performance,[12] using soft materials to improve durability,[23] and developing simple TENG structures to reduce fabrication costs.[24] However, because the three parameters have a trade-off relationship in terms of applicable fabrication

© 2022 Wiley-VCH GmbH

23669608, 2022, 7, Downloaded from https://onlinelibrary.wiley.com/doi/10.1002/smtd.202200248 by Korea Advanced Institute Of, Wiley Online Library on [21/11/2022]. See the Terms and Conditions (https://onlinelibrary.wiley.com/terms-and-conditions) on Wiley Online Library for rules of use; OA articles are governed by the applicable Creative Commons License

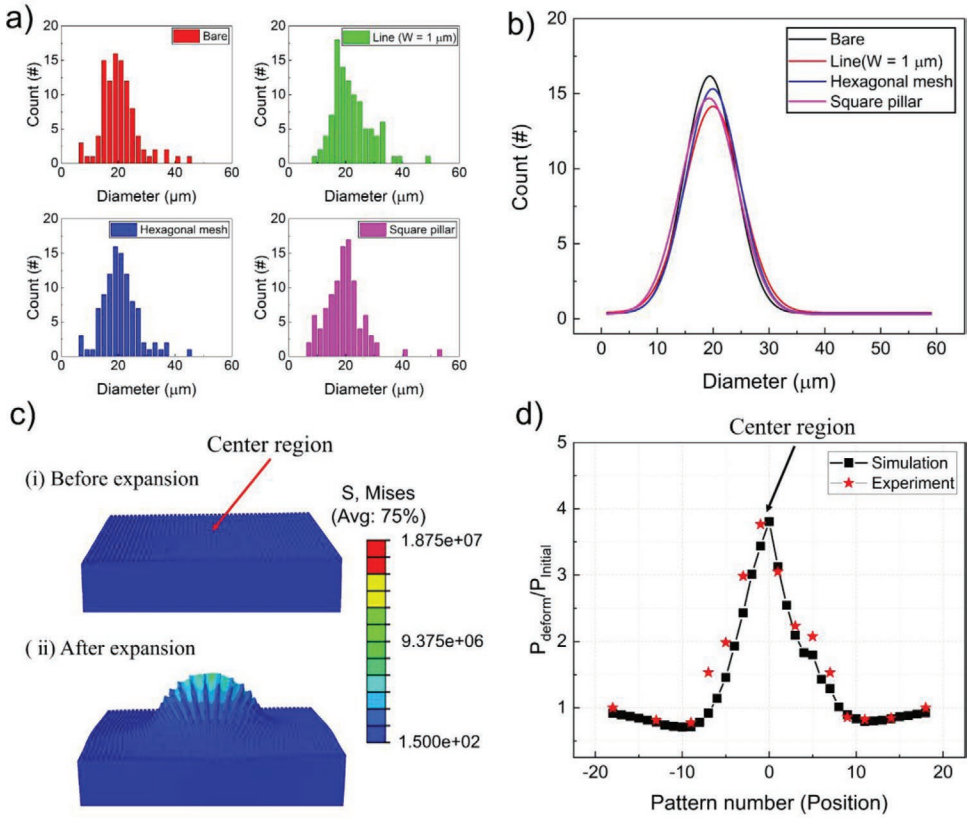


Figure 4. Size and Gaussian distributions of microstructures to verify the expansion capacity according to the nanopattern. a) Size distribution of the microstructures of the spherical micro/nano hierarchical structure (S-HS) with various types of nanopatterns. b) Gaussian distribution of the S-HSs with various types of nanopatterns. Regardless of the nanopattern, the microstructure size is distributed from 15 to 25 μm. c) Change in distance between the periodic nanopatterns after thermal expansion of the microspheres. d) Comparison of the numerical and experimental results. In this analysis, a line pattern with $W = 1$ μm was used and "P" means pitch between patterns.

methods, the researchers could independently achieve only one or two of these three objectives. Therefore, it still remains challenging to develop a TENG that satisfies all the above objectives.

To solve these problems, an S-HS was applied as a high-performance, mechanically durable, and low-cost TENG. First, as the TENG performance can be improved by increasing the roughness and surface area, it was reasonably expected that the developed S-HS could be used for a high-performance TENG. Second, by developing a fabrication method for forming S-HSs on highly deformable elastomeric substrates, high mechanical durability could be achieved because the damping effect by the viscoelastic behavior of the elastomer and the hemispherical shape could prevent stress concentration and mechanical oscillation under applied pressure or shock.[25] Third, because only high-throughput and low-cost fabrication processes were used to fabricate the S-HS, cost efficiency was also achieved. Accordingly, to verify the effects of the S-HS on the corresponding TENG, a contact-separation-mode device was fabricated and analyzed. In this experiment, the S-HS was used as the negative part of the TENG, and the nylon film was used as the positive part of the TENG, as shown in **Figure 5**a. Figure 5b presents the results of the experiments performed to evaluate the effects of the S-HS. When PDMS with 20 wt% microspheres and PDMS with a line pattern with $W = 1$ μm were used, 2.62 and 1.2 times higher triboelectric performance than that of the bare (flat) PDMS film was achieved, respectively. In addition, the triboelectric performance of S-HS based on a combination of microspheres and nanopatterns increased with the weight percentage of the microspheres, reaching a maximum at 20 wt%. The maximized TENG based on S-HS showed 4.48 times the triboelectric performance of the bare PDMS film owing to its high surface roughness and large surface area. Notably, we used the S-HS on only one side of the TENG to verify the structural effect clearly. Nevertheless, it is expected that higher performance will be obtained if S-HS is applied to both sides by changing the S-HS surface material.

Next, experiments were conducted to compare the various nanopatterns, as shown in Figure 5c. As reported previously,[12] the triboelectric performance changed less with the types of nanopatterns while the presence of nanopatterns makes a significant improvement in triboelectric performance. However, the nanoline pattern with $W = 200$ nm showed the lowest performance, whereas those with $W = 1$ μm exhibited the highest performance. These results are believed to be ascribed to the depth of the nanopattern. In the case of the nanoline pattern with $W = 200$ nm, the actual depth of PUA mold is relatively shallow compared to those with $W = 1$ μm as shown in Table S1 (Supporting Information), it was more difficult for the PDMS precursor to fill the PUA mold fully because of the narrow linewidth. In contrast, the mold of the line patterns

© 2022 Wiley-VCH GmbH

23669608, 2022, 7, Downloaded from https://onlinelibrary.wiley.com/doi/10.1002/smtd.202200248 by Korea Advanced Institute Of, Wiley Online Library on [21/11/2022]. See the Terms and Conditions (https://onlinelibrary.wiley.com/terms-and-conditions) on Wiley Online Library for rules of use; OA articles are governed by the applicable Creative Commons License

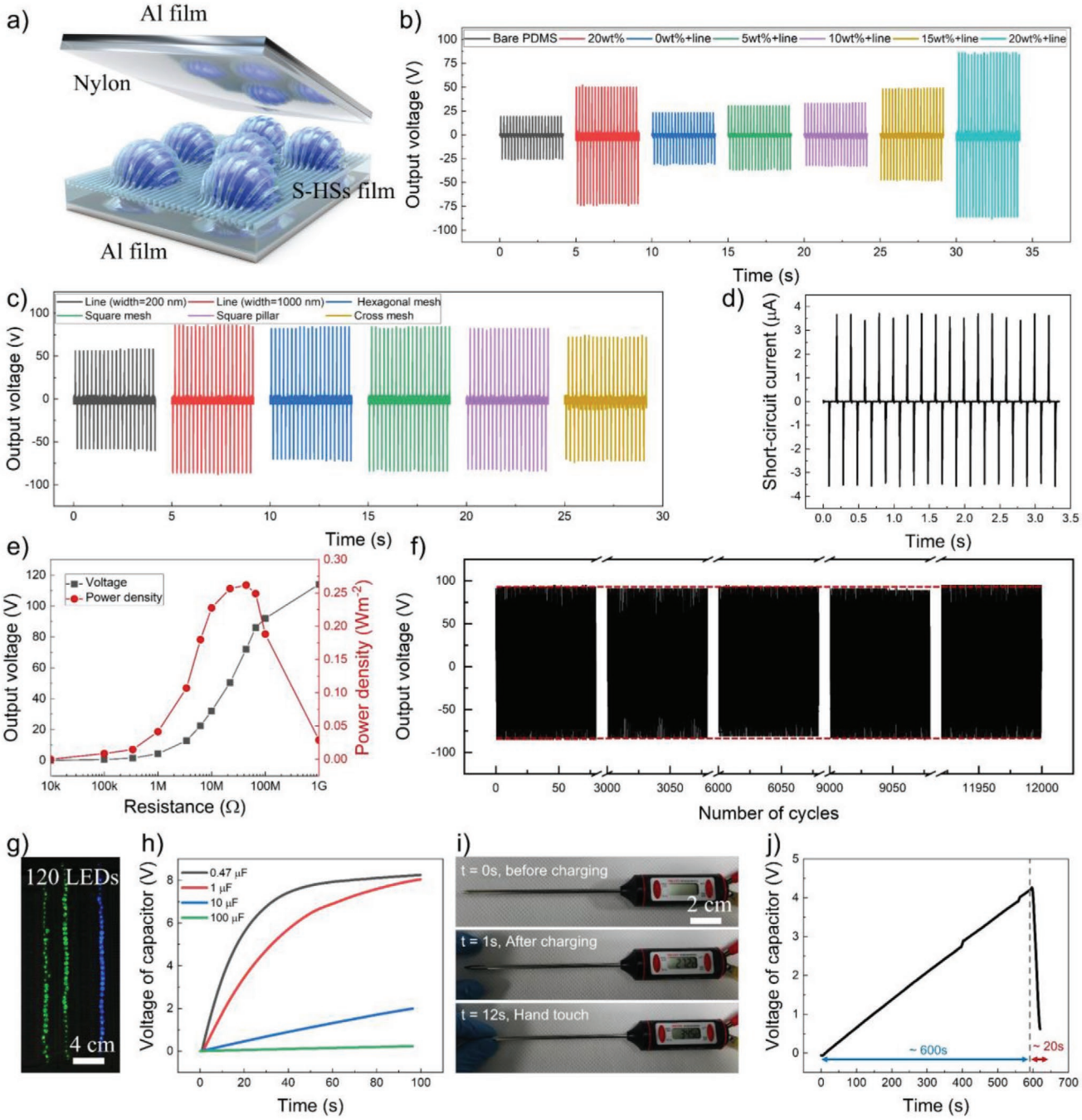


Figure 5. Application of spherical micro/nano hierarchical structure (S-HS) as a triboelectric nanogenerator (TENG). a) Schematic illustration of TENG based on S-HS. TENG output voltage of depending on the b) presence of micro- and nanopatterns and c) nanopattern shape. Results of the experiments for TENG characterization: d) short-circuit output current of TENG and e) TENG output voltage and power density in accordance with the applied external resistance. f) TENG output voltage during repeated 12 000 cyclic tests. g) Photographic image of 120 LEDs powered by the TENG under an input frequency of 5 Hz and h) charged voltages of the capacitors depending on the charging time under an input frequency of 10 Hz. i) Photographs of the commercialized thermocouple at 0, 1, and 12 s after connecting with the charged capacitor. j) Capacitor voltage during charging for 600 s by the TENG and discharging for 20 s by the thermocouple.

with $W = 1$ μm had the largest linewidth and highest trench (1 μm in height), forming a clearly textured surface, which could increase the effective surface area. Additional experiments were conducted to characterize the TENG using line patterns with $W = 1$ μm. As shown in Figure 5d,e, the short-circuit current was 3.71 μA and the maximum power density was 0.262 Wm^{-2}. In addition, the enhanced performance was maintained without degradation during 12 000 cyclic

© 2022 Wiley-VCH GmbH

23669608, 2022, 7, Downloaded from https://onlinelibrary.wiley.com/doi/10.1002/smtd.202200248 by Korea Advanced Institute Of, Wiley Online Library on [21/11/2022]. See the Terms and Conditions (https://onlinelibrary.wiley.com/terms-and-conditions) on Wiley Online Library for rules of use; OA articles are governed by the applicable Creative Commons License

tests and there are no structural changes to the spherical structures after the cyclic tests owing to its high mechanical durability, as shown in Figure 5f and Figure S6 (Supporting Information). Additional detailed characterizations, such as the output charge density and triboelectric performance in accordance with the input frequency and force, are described in Figure S7 (Supporting Information). Finally, the developed TENG was used to turn on the LEDs and to charge the capacitors for driving a commercialized thermocouple, as shown in Figure 5g–j. A total number of 120 LEDs were successfully powered by the TENG with just a rectifier as shown in Video S1 (Supporting Information). In addition, by charging the capacitor at 100 μF for 600 s, the thermocouple was driven for 20 s and the temperature of a human hand was successfully measured, as shown in Video S2 (Supporting Information). In summary, it was demonstrated that a TENG achieving all the above key objectives, namely, high performance, high mechanical durability, and a low-cost process, was successfully realized using the proposed S-HS.

2.5. Application of S-HS to Sustainable Water Harvesting

Second, we present another promising application of the proposed S-HS with high surface area and hydrophobicity by demonstrating a water harvesting device (**Figure 6**). With the rapid development of the world economy, water shortage is becoming a severe issue all over the world. Interestingly, a variety of natural creatures efficiently capture water in a fog environment, which can provide an inspiration to develop facile and novel water harvesting devices.[26] For example, the Namib beetle efficiently harvests water in a fog environment using a spherical structure (i.e., bump topography) formed on its back and covered with hydrophobic wax.[27] In addition, the convex spherical structure can localize the droplet growth by concentrating the vapor diffusion flux, significantly enhancing the water condensation performance.[28–30] As a spherical structure can easily be manufactured on the surface of the proposed S-HS and it consists of PDMS, which is hydrophobic, we used the S-HS for efficient water condensation. Figure 6a shows the core concepts for the growth and transport of water droplets. In the fog environment, vapor diffusion flux is formed (Figure 6a(i)). The nucleation begins on the S-HS surface (Figure 6a(ii)). Small nuclei grow to form microscale droplets through coalescence (Figure 6a(iii)). With continued water condensation, microscale droplets continuously grow to form large droplets, and the large droplets roll from the surface. After the surface is regenerated (Figure 6a(iv)), the same processes (i–iv) are repeated. Figure 6b shows the experimental setup based on the Peltier module, humidifier, and chamber. The sample plate temperature was maintained at 12 ± 0.3 °C (Figure S8, Supporting Information). The humidifier was placed 10 cm away from the sample plate and the collected water was gathered in a vial placed under the sample plate. We recorded time-lapse images of the formation of microscale droplets on the S-HS (Figure 6c(i)). To check the growth mechanism on the surface, S-HS with 5 wt% of microspheres and a line pattern with $W = 1$ μm was used in this experiment. In the S-HS area, the droplets grew more substantially and a relatively larger size of water droplets was generated compared to the nanostructure-only surfaces. (Figure 6c(ii)). These results mean that the S-HS increased the effective surface area and concentrated the vapor diffusion flux at top of the spherical structure. Figure S9a,b (Supporting Information) shows the change in the contact angle caused by varying the surface. With a bare PDMS, the measured contact angle was only 110.5°. When the microsphere concentration was increased, the contact angles rapidly increased, showing the highest contact angle of 151.0° with 20 wt% microspheres and a line pattern. In addition, we compared the water contact angles with the different nanopattern types. The contact angles were similar except in the case of the nanoline pattern with $W = 200$ nm. We also examined the water condensation performance of different surfaces (Figure 6d–f). Firstly, the water collection rate is defined as the weight of collected water per hour divided by the sample size. We measured the water condensation performance on the different surfaces including bare, nanostructure only (0 wt% + line), microstructure only (20 wt%), and S-HS different microsphere concentrations (Figure 6d). The PDMS with 20 wt% microspheres and PDMS with a line pattern with $W = 1$ μm showed 5 and 2.5 times higher water condensation performance than that of the bare (flat) PDMS film. In addition, as the microsphere concentrations within the S-HSs with nanoline patterns increased, the water condensation performance increased and reached a maximum with a microsphere concentration of 20 wt%. The maximized water condensation performance of the S-HS was eight times higher than that of the bare PDMS because of the elevated surface area and roughness. We additionally conducted water condensation tests to compare the performance with various nanopatterns, as shown in Figure 6e. The nanoline pattern with $W = 200$ nm yielded the lowest water condensation performance, whereas the other patterns exhibited similar performances. In particular, the line pattern with $W = 1$ μm showed the highest performance due to the high nanopattern height. For the S-HS to be used in practical water condensation applications, condensation performance should be maintained for a time long period under high humidity environment. Therefore, we checked the water condensation performance of the S-HS over 7 days and similar water collection rates were consistently measured throughout repeated water condensation tests (Figure S10, Supporting Information). In addition, we also used 3D profile results to examine the surface of the S-HS, for which was used in a water condensation test for 7 days. The 3D profile results showed approximately similar tendencies. The spherical microstructures had no significant structural change. The average and standard deviation of the spherical microstructures' sizes were measured as 21.9 ± 6.9 μm before test and 21.1 ± 7.4 μm after test (Figure S11, Supporting Information). Finally, we verified the effect of the direction of the nanopatterns (Figure 6f). The line patterns with the vertical direction (i.e., along the direction of gravitational force) exhibited higher performance than the horizontal direction (i.e., perpendicular direction to the gravitational force). This result is believed to be ascribed to the role of nanostructures. The difference in the water condensation performance of the mounting directions can be attributed to the sliding effect of water droplets. The nanostructure of the surface causes a sliding effect so that the grown water droplets easily roll off from the surface of the

© 2022 Wiley-VCH GmbH

23669608, 2022, 7, Downloaded from https://onlinelibrary.wiley.com/doi/10.1002/smtd.202200248 by Korea Advanced Institute Of, Wiley Online Library on [21/11/2022]. See the Terms and Conditions (https://onlinelibrary.wiley.com/terms-and-conditions) on Wiley Online Library for rules of use; OA articles are governed by the applicable Creative Commons License

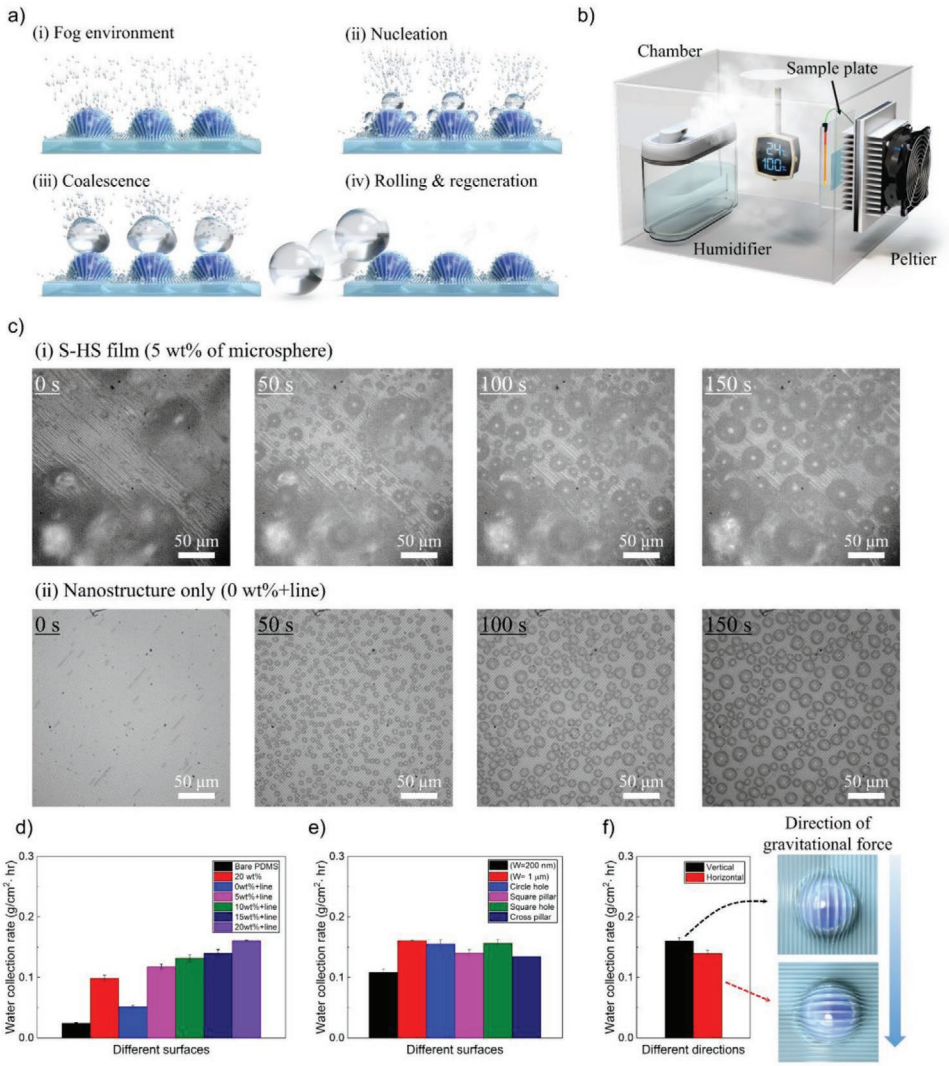


Figure 6. Application of spherical micro/nano hierarchical structure (S-HS) for water harvesting. a) Central concepts for the growth and transport of water droplets on the S-HS surface. b) Experimental setup based on a Peltier module, humidifier, and chamber. c) Time-lapse imaging of the formation of microscale droplets on S-HS and nanostructure-only surface. In this experiment, a line pattern with $W = 1$ μm and S-HS with 5 wt% of microsphere concentration and nanostructure-only surface with $W = 1$ μm were used to observe the water droplet formation on the surface. In the S-HS, a relatively larger size of water droplets was generated compared to the nanostructure-only surface. d–f) Water condensation performance on different surfaces with different microsphere concentrations and the line pattern with $W = 1$ μm (d), different types of nanopatterns (e), and direction of nanopatterns (f). The nanopattern on the surface undergoes a sliding effect, so the grown water droplets easily and quickly roll off from the surface of the S-HS, and the water collection rate is improved on the surface with the vertical patterns.

S-HS, improving the performance in the vertical direction. These results demonstrate that the fabricated S-HS is capable of water harvesting with high condensation performance.

3. Conclusion

In this study, a novel approach was developed for the facile and scalable fabrication of 3D S-HS-based flexible elastomers using and nanopatterned structures and thermally expandable microspheres. By transferring the composite and applying thermal expansion treatment, we fabricated S-HS over a large area and controlled the geometrical parameters of the micro/nanostructures. Using this approach, S-HS with various nanopatterns and a controlled density of microstructures was created with well-designed primary microstructures and periodic secondary nanostructures. Thermally expandable microspheres can easily and quickly generate spherical microstructures on a large scale. Through experiments and FEM simulations, we demonstrated the expansion mechanism of the 3D spherical microstructure. Using this method, we demonstrated that various types of nanopatterns and the density of the spherical microstructures can be quantitatively controlled, enabling an increased surface area and mechanical durability. Given these advantages, the developed S-HS was applied to achieve high-performance, mechanically durable, low-cost TENGs. The TENG based on S-HS exhibited 4.48 times higher triboelectric performance than the TENG with bare PDMS film. Finally, the capability of the fabricated S-HS for

© 2022 Wiley-VCH GmbH

23669608, 2022, 7, Downloaded from https://onlinelibrary.wiley.com/doi/10.1002/smtd.202200248 by Korea Advanced Institute Of, Wiley Online Library on [21/11/2022]. See the Terms and Conditions (https://onlinelibrary.wiley.com/terms-and-conditions) on Wiley Online Library for rules of use; OA articles are governed by the applicable Creative Commons License

water harvesting systems was demonstrated. The S-HS successfully collected water from the fog owing to its increased surface area and spherical microstructures. We believe that the demonstrated S-HS approach opens a new route for the fabrication of hierarchical structures in renewable electrical energy harvesting and sustainable water harvesting applications with high performance. We expect that our study will present a new avenue toward advanced hierarchical structures for real-life applications such as sensing devices, energy harvesting, chemical sensing, and microlens array.

4. Experimental Section

Fabrication of Nanopatterned Molds: Nanopatterned PUA molds were fabricated using conventional UV-nanoimprint lithography. To fabricate the molds, a Si master was prepared using krypton fluoride lithography and e-beam lithography. For polymer mold replication, RM-311 resin (polyurethane, Minuta Technology Co., Ltd., Korea) was poured onto the prepared Si master and covered with UV-transparent polyethylene terephthalate film. Pressure was applied to the resin using a hand roller to facilitate the complete penetration of the resin into the nanopatterns of the Si master. Then, the resin was cured under UV illumination for 3 min and separated from the Si master. This process can be conducted repeatedly, and various nanopatterns can be fabricated using various Si masters. The detailed fabrication process of the polymer mold from the Si master is described in our previous report.[31,32] Note that the surface of the Si master and PUA had to be treated with trichloro(1H, 1H, 2H, 2H-perfluorooctyl)silane to facilitate the detachment of the polymer mold and PDMS.

Fabrication of the S-HS: Firstly, thermally expandable microspheres (MSH-550, SDI Korea, Korea) were added to the well-mixed liquid PDMS precursor (Sylgard 184, Dow Corning Corp., USA), in which the resin and hardener were mixed in a 10:1 weight ratio. For uniform mixing and degassing, the PDMS/microsphere precursor was mixed for 2 min using a planetary mixer (THINKY, ARE-310). Then, it was poured into the PUA mold. Pressure was applied to the mixture using a hand roller to facilitate the complete penetration of this mixture into the nanopatterns of the PUA mold. Thermal curing was then performed at 80 °C for 4 h. The cured composite film was peeled off from the mold and heated at 180 °C for 3 min, where the microsphere expansion was maximized.

Characteristics of S-HS: The morphology of the S-HS was characterized via FE-SEM. The surface and morphology of the hierarchical structure were characterized using a confocal laser microscope (VX-X1050, KEYENCE, Japan). The finite element method was employed in conjunction with Abaqus software to calculate the changed distance between the nanopatterns after the expansion of the microspheres.

S-HS TENG Characterization: A TENG with dimensions of 3 × 3 cm was used. A digital oscilloscope (DPO2002B, Tektronix, USA), voltage probe with an input impedance of 40 MΩ (P5100A, Tektronix, USA), and pre-current amplifier (SR570, Stanford Research Systems, USA) were used to measure the output voltage and current. A system electrometer (Model 6514, Keithley Instrument, USA) was used to measure the output voltage, current, and transferred charge. A dual-channel arbitrary/function generator (AFG3022, Tektronix, USA) was employed to generate a sinusoidal function for shaker excitation. To drive the shaker, a higher voltage and current were required; thus, a power amplifier (Type BAA 120, TIRA, Germany) was used. A vibration test system (TV 51 075, TIRA, Germany) was employed as a shaker to demonstrate the contact-separation-mode TENG. For contact force measurement, a force sensor (1051V2, Dytran Instruments, USA) was used and powered by a sensor signal conditioner (Model 480E09, PCB Piezotronics, USA). The output triboelectric performance of the TENG was investigated at different forces (2, 4, 6, 8, and 10 N) and frequencies (1–5 Hz). Thereafter, the operating force and frequency were selected to be 8 N and 5 Hz, respectively, to characterize the triboelectric performance of the TENG.

S-HS Water Condensation Characterization: A water harvester with dimensions of 3 × 3 cm was used. The substrates were treated with a self-assembled monolayer (trichloro(1H, 1H, 2H, 2H-perfluorooctyl)silane; Sigma-Aldrich, USA) to increase the hydrophobicity of the PDMS surface. The water contact angles were measured using a Contact Angle Meter (DO4010, Kruss GmbH, Germany). A 10 µL droplet of deionized water was placed on the surface of each sample. Figure S12 (Supporting Information) shows the experimental setup of the microscopic condensation. The S-HSs were placed on the temperature-humidify controlled stage connected to a water-saturated nitrogen flow. The condensation behaviors were observed using high-speed microscopy (Miro M110 Phantom, AMETEK, USA) connected to a microscope (BX53, Olympus, Japan). The environmental temperature, sample plate temperature, and relative humidity were maintained as 22 ± 2 °C, 12 ± 0.3 °C, and 90 ± 2%, respectively. For feedback control of the surface temperature of the sample and chamber temperature, the temperatures were measured and recorded by a data logger (midi LOGGER GL220, Graphtec, Japan) and were controlled using proportional–integral–derivative control by Arduino. The level of supersaturation was set to be ≈1.6 throughout all the experiments. The fabricated S-HS was placed on the sample plate perpendicular to the fog flow direction in order to capture the water directly and in real-time.

Supporting Information

Supporting Information is available from the Wiley Online Library or from the author.

Acknowledgements

This research was supported by the National Research Foundation of Korea (NRF) grant funded by the Korea government (MSIT) (No. 2021R1A2C3008742), Basic Science Research Program through the National Research Foundation of Korea (NRF) funded by the Ministry of Education (No. 2021R1I1A1A01051208), the Center for Advanced Meta-Materials (CAMM) funded by the Ministry of Science, ICT and Future Planning, Korea, through the Global Frontier Project (CAMM-No. 2014M3A6B3063707), and the Technology Development Program (3104117) funded by the Ministry of SMEs and Startups (MSS, Korea), Korea.

Conflict of Interest

The authors declare no conflict of interest.

Author Contributions

Y.J. and J.A. contributed equally to this paper. The manuscript was written through the contributions of all authors. All authors have given approval to the final version of the manuscript.

Data Availability Statement

Research data are not shared.

Keywords

hierarchical structures, microspheres, nanopatterns, triboelectric nanogenerators, water condensation

Received: February 28, 2022
Revised: April 2, 2022
Published online: May 4, 2022

© 2022 Wiley-VCH GmbH

23669608, 2022, 7, Downloaded from https://onlinelibrary.wiley.com/doi/10.1002/smtd.202200248 by Korea Advanced Institute Of, Wiley Online Library on [21/11/2022]. See the Terms and Conditions (https://onlinelibrary.wiley.com/terms-and-conditions) on Wiley Online Library for rules of use; OA articles are governed by the applicable Creative Commons License

[1] H. G. Andrews, E. A. Eccles, W. C. E. Schofield, J. P. S. Badyal, *Langmuir* **2011**, *27*, 3798.
[2] W. K. Lee, W. Bin Jung, S. R. Nagel, T. W. Odom, *Nano Lett.* **2016**, *16*, 3774.
[3] Y. Zhang, S. Ma, B. Li, B. Yu, H. Lee, M. Cai, S. N. Gorb, F. Zhou, W. Liu, *Chem. Mater.* **2021**, *33*, 2785.
[4] K. Liu, J. Du, J. Wu, L. Jiang, *Nanoscale* **2012**, *4*, 768.
[5] Y. T. Cheng, D. E. Rodak, *Appl. Phys. Lett.* **2005**, *86*, 144101.
[6] H. Gao, L. Zhao, L. Wang, P. Sun, H. Lu, F. Liu, X. Chuai, G. Lu, *Sens. Actuators, B* **2018**, *255*, 3505.
[7] Y. Song, W. Wang, L. Ge, X. Xu, Z. Zhang, P. S. B. Julião, W. Zhou, Z. Shao, *Adv. Sci.* **2017**, *4*, 1700337.
[8] A. Fernández, A. Francone, L. H. Thamdrup, A. Johansson, B. Bilenberg, T. Nielsen, M. Guttmann, C. M. Sotomayor Torres, N. Kehagias, *J. Micromech. Microeng.* **2017**, *27*, 045020.
[9] A. M. Brzozowska, S. Maassen, R. Goh Zhi Rong, P. I. Benke, C. S. Lim, E. M. Marzinelli, D. Jańczewski, S. L. M. Teo, G. J. Vancso, *ACS Appl. Mater. Interfaces* **2017**, *9*, 17508.
[10] Y. Tian, L. Jiang, *Nat. Mater.* **2013**, *12*, 291.
[11] B. Dudem, Y. H. Ko, J. W. Leem, J. H. Lim, J. S. Yu, *ACS Appl. Mater. Interfaces* **2016**, *8*, 30165.
[12] J. Ahn, Z. J. Zhao, J. Choi, Y. Jeong, S. Hwang, J. Ko, J. Gu, S. Jeon, J. Park, M. Kang, D. V. Del Orbe, I. Cho, H. Kang, M. Bok, J. H. Jeong, I. Park, *Nano Energy* **2021**, *85*, 105978.
[13] X. Yan, F. Chen, S. Sett, S. Chavan, H. Li, L. Feng, L. Li, F. Zhao, C. Zhao, Z. Huang, N. Miljkovic, *ACS Nano* **2019**, *13*, 8169.
[14] J. Feng, M. T. Tuominen, J. P. Rothstein, *Adv. Funct. Mater.* **2011**, *21*, 3715.
[15] J. Shao, Y. Ding, W. Wang, X. Mei, H. Zhai, H. Tian, X. Li, B. Liu, *Small* **2014**, *10*, 2595.
[16] A. K. Kota, Y. Li, J. M. Mabry, A. Tuteja, *Adv. Mater.* **2012**, *24*, 5838.
[17] W. Zhang, M. Li, Q. Wang, G. Chen, M. Kong, Z. Yang, S. Mann, *Adv. Funct. Mater.* **2011**, *21*, 3516.
[18] H. Tian, J. Shao, H. Hu, L. Wang, Y. Ding, *ACS Appl. Mater. Interfaces* **2016**, *8*, 16419.
[19] Y. Lin, R. Zhou, J. Xu, *Adv. Mater. Interfaces* **2018**, *5*, 1801126.
[20] R. Lei, Y. Shi, Y. Ding, J. Nie, S. Li, F. Wang, H. Zhai, X. Chen, Z. L. Wang, *Energy Environ. Sci.* **2020**, *13*, 2178.
[21] J. S. Kim, J. Kim, J. N. Kim, J. Ahn, J. H. Jeong, I. Park, D. Kim, I. K. Oh, *Adv. Energy Mater.* **2022**, *12*, 2103076.
[22] Y. Zou, J. Xu, K. Chen, J. Chen, *Adv. Mater. Technol.* **2021**, *6*, 200091622.
[23] Z. Lin, B. Zhang, Y. Xie, Z. Wu, J. Yang, Z. L. Wang, *Adv. Funct. Mater.* **2021**, *31*, 1502566.
[24] Y. Li, Z. Zhao, Y. Gao, S. Li, L. Zhou, J. Wang, Z. L. Wang, *ACS Appl. Mater. Interfaces* **2021**, *13*, 30776.
[25] Z. J. Zhao, J. Ahn, S. H. Hwang, J. Ko, Y. Jeong, M. Bok, H. J. Kang, J. Choi, S. Jeon, I. Park, J. H. Jeong, *ACS Nano* **2021**, *15*, 503.
[26] H. Zhu, Z. Guo, W. Liu, *Chem. Commun.* **2016**, *52*, 3863.
[27] J. Lei, Z. Guo, *Nanoscale* **2020**, *12*, 6921.
[28] J. K. Park, S. Kim, *Micromachines* **2019**, *10*, 201.
[29] Y. Yao, J. Aizenberg, K. C. Park, *Appl. Phys. Lett.* **2018**, *112*, 151605.
[30] K. C. Park, P. Kim, A. Grinthal, N. He, D. Fox, J. C. Weaver, J. Aizenberg, *Nature* **2016**, *531*, 78.
[31] Z.-J. Zhao, J. Ahn, D. Lee, C. B. Jeong, M. Kang, J. Choi, M. Bok, S. Hwang, S. Jeon, S. Park, J. Ko, K. S. Chang, J.-W. Choi, I. Park, J.-H. Jeong, *Nanoscale* **2022**, *14*, 1136.
[32] Z. J. Zhao, J. Ahn, J. Ko, Y. Jeong, M. Bok, S. H. Hwang, H. J. Kang, S. Jeon, J. Choi, I. Park, J. H. Jeong, *ACS Appl. Mater. Interfaces* **2021**, *13*, 3358.

© 2022 Wiley-VCH GmbH

23669608, 2022, 7, Downloaded from https://onlinelibrary.wiley.com/doi/10.1002/smtd.202200248 by Korea Advanced Institute Of, Wiley Online Library on [21/11/2022]. See the Terms and Conditions (https://onlinelibrary.wiley.com/terms-and-conditions) on Wiley Online Library for rules of use; OA articles are governed by the applicable Creative Commons License